

Evaluation of the Atmospheric Correction Procedure for the APEX Level 2/3 Processor

Daniel Schlöpfer ^a, Jan Biesemans ^b, Andreas Hueni ^a, and Koen Meuleman ^b

a) Remote Sensing Laboratories (RSL), Dept. of Geography, Univ. of Zürich, Switzerland

daniel@rese.ch; ahueni@geo.uzh.ch

b) VITO, Mol, Belgium

jan.biesemans@vito.be, koen.meuleman@vito.be

ABSTRACT

The Airborne Prism Experiment (APEX) is a hyperspectral instrument built in a Swiss - Belgian collaboration within the ESA-PRODEX program [1]. It aims at highest possible accuracy of its delivered surface reflectance image data products. The atmospheric correction of hyperspectral imagery is a critical element of a complete processing chain towards unbiased reflectance and for the creation of higher level products. As the first data of APEX is expected to become available in 2009, an appropriate processing chain for higher level processing needs to be defined and evaluated. Standard products have been identified in all application fields of hyperspectral imaging, i.e., geology, vegetation, cryosphere, limnology and atmosphere. They are being implemented at the APEX science center [2]. The according processing procedures rely on data of well-defined processing states which range from calibrated at-sensor radiance to (bihemispherical) spectral albedo.

In this paper, the atmospheric processing which is implemented as part of the automated data processing chain for level 2 in the APEX processing and archiving facility (PAF) [3] is evaluated together with the ATCOR-4 atmospheric correction program [4],[5]. The evaluation is done regarding flexibility, reflectance output accuracy and processing efficiency. Two test data sets are taken for this purpose: a well-documented set of HYMAP data [6] and a high resolution HYSPEX data set [7]. Both data sets exhibit areas of overlap, which are taken for self-contained analysis of the atmospheric correction procedure. The accuracy tests include plausibility checks on selected regions of interest including a variety of known surfaces in the imagery. As some of the observed effects are related to BRDF differences, the results also give an indication for the inaccuracy related to these reflectance anisotropies. Speed measurements of the processing are then compared to the demand for operational processing of series of data acquisition. Further comparison information is drawn from the by-products of atmospheric correction such as water vapor distribution maps.

The study shows performance and limitations of atmospheric correction using the state-of-the-art technology, which are mainly found in the field of BRDF effects. This points towards improvements to be implemented in course of the further development of the higher level processing chain for the APEX sensor.

1. INTRODUCTION

Atmospheric correction of hyperspectral imagery is a topic whose physics are well known but whose implementation has to deal with the solution and interpolation of (at least) 6 parameters, i.e., the wavelength, the surface reflectance, the adjacency reflectance, the water vapor, the aerosol contents, and the terrain altitude and slope. For APEX, existing routines are to be adapted to perform well for high spatial and spectral resolution at the same time. Recent experience at the Remote Sensing Laboratories Zürich has shown that the surface reflectance retrieval with existing high resolution imaging spectrometers such as AISA (Specim) or HYSPEX is still a topic to be investigated and improved in future developments, specifically if the data is to be used in conjunction with other data sources [9].

The atmospheric correction has to be implemented in a flexible way such that it can be adapted to the needs of higher level product generation routines. The requirements regarding reflectance accuracy are high because APEX shall also serve as cross-calibration tool for space instruments. The respective accuracies of better than 1% in absolute reflectance are difficult to achieve due to the fact that APEX offers spectral resolutions down to 1 nm in the visible spectral range at spatial resolutions between 1 and 3 meters. The performance of the instrument shall be achievable over dark surfaces

such as lakes as well as over bright areas, e.g. snow. Another critical requirement for atmospheric correction is the computing efficiency. It is necessitated by the huge data amounts to be processed by time consuming calculations. The goal is to deliver processed data acquired during a typical flight campaign within 24 hours. Utilising parallel processing is inevitable to meet these time requirements.

2. METHODS

The atmospheric correction processing evaluated within this paper is to a major part based on the technology of the ATCOR-4 atmospheric correction procedure [4],[5]. This program is one of the established standards for atmospheric correction of hyperspectral imagery. It follows a physical approach by inverting the MODTRAN-4 radiative transfer code and includes the correction for terrain influences, adjacency effects, spatial water vapor distribution, aerosol content variations and variation of diffuse illumination. The original implementation uses a pre-compiled look-up-table (LUT) for this inversion. As the technology has been published elsewhere, no further details regarding the atmospheric correction procedure are given in this paper.

In support of (a) the recurrent hyperspectral campaigns (<http://campaigns.vgt.vito.be/>), (b) the design of new airborne (e.g. <http://medusa.vgt.vito.be/>) and spaceborne camera systems and (c) to enhance the scientific experimentation within an operational setting, the Flemish Institute for Technological Research (VITO) has developed a dedicated experimental Central Data Processing Center (CDPC) for airborne and spaceborne earth observation [11]. The algorithms integrated in the CDPC are all VITO-developed C++ implementations of commonly accepted image processing algorithms. With respect to atmospheric correction the following methodologies are implemented:

- The MODTRAN4 interrogation technique as described in de Haan and Kokke [12] has been used. VITO does not use the traditional approach of a precompiled LUT (although this option still exists), but the CDPC performs the MODTRAN4 configuration and execution “on the fly”. As such, all 176 MODTRAN4 configuration parameters are principally available for the researcher (using ATCOR, there are only some major parameters available: sensor elevation, ground topography, solar zenith, sensor view angle, water vapor, visibility, and aerosol type). During the image processing MODTRAN4 configuration files are created, the needed parameters are determined by the given image geometry, possible in-situ measurements and the meteorological conditions (e.g. cloud cover, O₃ content, or CO₂ content), the MODTRAN4 runs are performed and finally the MODTRAN4 output is used to calculate the atmospheric correction.
- Haze removal, shadow removal and topographic BRDF are based on the methodology described in Richter [5].
- Visibility extraction is based on Richter [13].
- Water vapor extraction algorithm is implemented according to Rodger [14].
- Atmospheric BRDF correction can be enforced by configuring the CDPC to do view-zenith dependent MODTRAN4 simulations.
- Target BRDF correction according the kernel BRDF correction algorithms described in Jupp [15].

The current version of the CDPC does not allow for noise reduction filtering or spectral polishing filtering (the latter are often used to remove the ‘spikes’ in the water absorption area).

Hereafter, this collection of VITO implementations is named ‘CDPC’ and is validated together with the original implementation of ATCOR-4. For this validation exercise, the haze removal, shadow removal, atmospheric BRDF and target BRDF algorithms were not activated

3. DATA BASIS

Two data sets have been selected for an in-depth analysis of the correction performance on real data, a scene based on HYMAP data and a second scene using HYSPEX data. This paper focuses primarily on the first set, as it is better documented by in-situ ground measurements and surface spectra. Both data sets have been orthorectified using PARGE and the overlap area is derived by mosaicing two adjacent scenes.

3.1 HYMAP

The scene 'Vordemwald' is a HYMAP research data set, acquired in conjunction with extensive field data acquisition. It spans over hilly terrain and contains a wide variety of partially spectroradiometrically measured validation targets (e.g., vegetation, agriculture, water, settlements). The test data consists of two adjacent scenes which are mosaiced on the same DEM (see Figure 1). The DEM stems from laser scanning data and topographic maps for the upper part of the image. It has been smoothed to 5 m spatial resolution. Radiometric gain and offset of the imagery is provided separately after data acquisition and has been derived from inflight calibration in conjunction with laboratory reference data. The total FOV of this whiskbroom type of scanner is 61.4° , which is large if compared to APEX (28°). Further meta data for the two scenes are given in Table 1 below.

Table 1 Information for test HYMAP data set 'Vordemwald'.

Scene	Date	Local Time	Solar Zenith	Solar Azimuth*	Flight Heading*	Flight Altitude [m]	Ground elevation
run 1	29/07/2004	9:25:50	38.8°	126.2°	179.96°	2880m	473m
run 2	29/07/2004	9:33:00	37.9°	128.4°	0.21°	2890m	481m

* north: 0° , east: 90° .

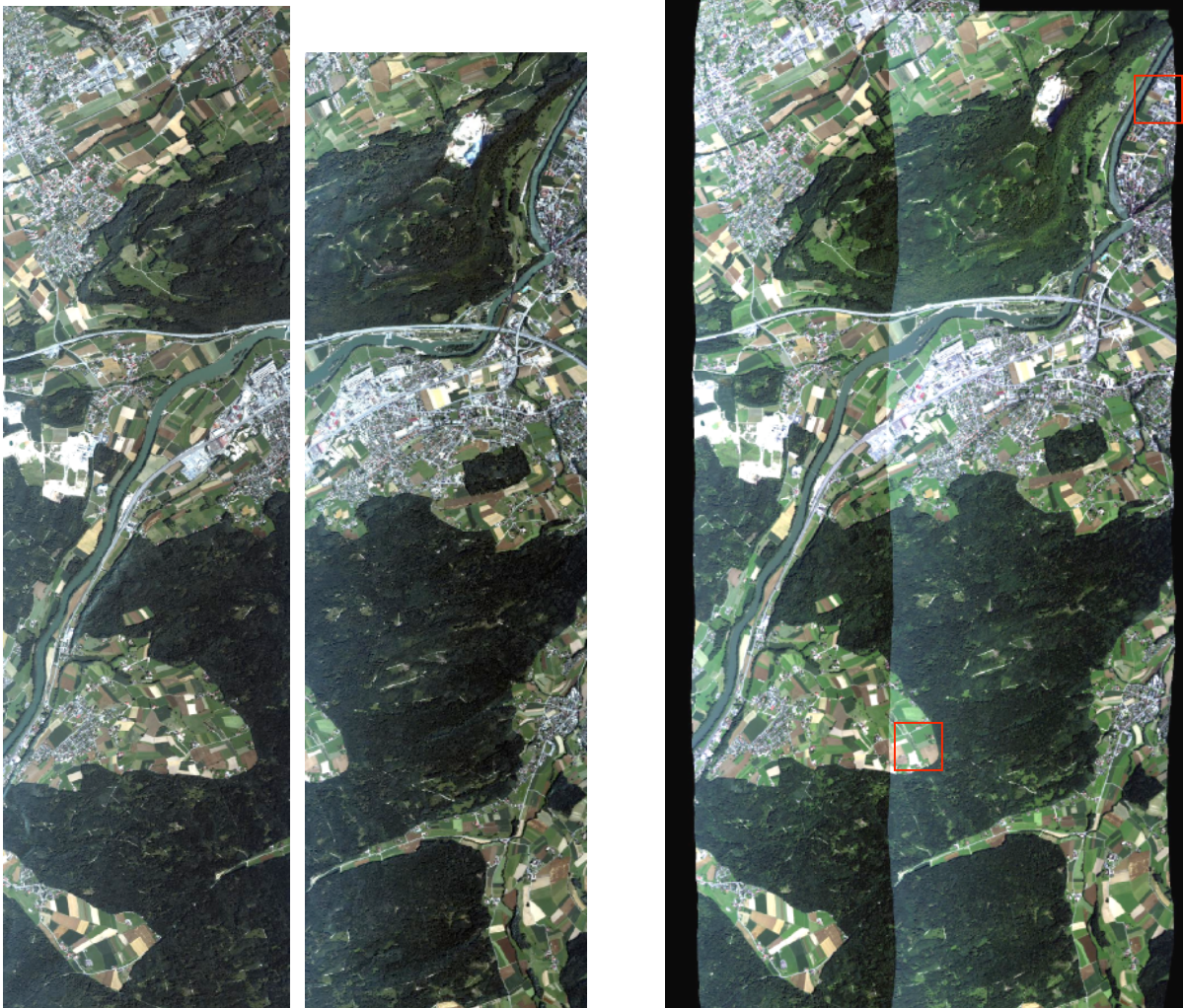


Figure 1 HYMAP data set 'Vordemwald' (Switzerland, 2004). Two flight strips and overlay of the two strips in a mosaic after PARGE orthorectification. Red: ground spectral measurement positions (data in courtesy of RSL, Zürich).

3.2 HYSPEX

Two HYSPEX scenes have been selected for image-based validation. They offer 1600 across track pixels at 4000 image lines imaged with a total FOV of 16.8° (which is lower than the APEX total FOV of 28°). HYSPEX scans at high spectral resolution in the VNIR spectral range between 408 and 985 nm in 160 spectral bands (i.e., ~ 3.5 nm spectral resolution, see [7] and [8] for more detail). For the VNIR part, this dataset is close to the specifications of the APEX system. Therefore, one of the strips serves as a large test cube for the APEX PAF. The instantaneous field of view is ~ 0.19 mrad across track and 0.38 mrad along track, corresponding to $\sim 30 \times 60$ cm pixel size for the given low altitude. The scan rate of the camera was set for each flight line to roughly match the along track pixel size for the real flight parameters (e.g. altitude and ground speed). A laser scanner DSM and DEM has been acquired simultaneous to the data acquisition for highest possible orthorectification accuracy. A subset of the imagery is shown in Figure 2, whereas the meta data for the two strips are given in Table 2.

Table 2 Information for test HYSPEX data set 'Biokal'.

Scene	Date	Local Time	Solar Zenith	Solar Azimuth	Flight Heading	Flight Altitude [m]	Ground elevation
run 1_2	16/07/2007	9:52:04	53.5°	113.1°	113.1°	1730m	290m
run 1_3	16/07/2007	9:55:54	53.2°	113.8°	-27.0°	1715m	310m

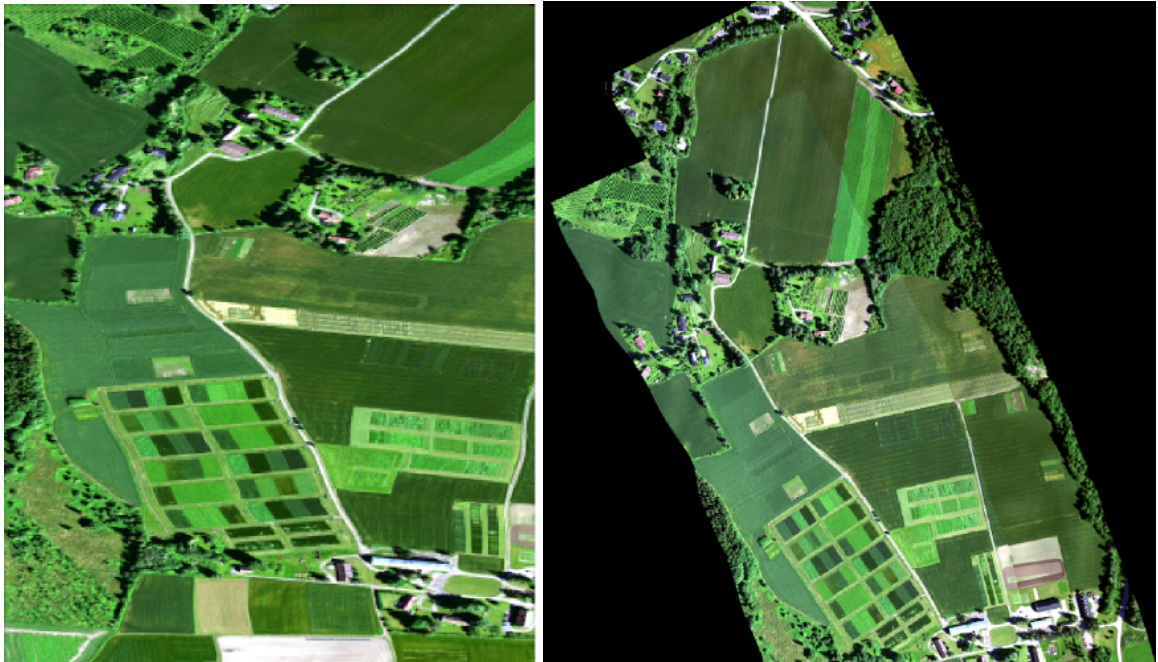


Figure 2 Subset of HYSPEX data set 'Biokal', Norway, 2007, before (left) and after processing to a mosaic (right); (data in courtesy of Norsk Elektro Optikk, Norway).

4. ATMOSPHERIC CORRECTION RESULTS

The results of the atmospheric correction are compared on the basis of the reflectance values which are produced by the atmospheric correction. For direct comparison, the calibrated uncorrected radiance values L_s are converted to apparent reflectances ρ_{app} by:

$$\rho_{app} = \frac{\pi L_s}{E_0 \cos \theta_s} \cdot 100\% = \frac{\pi (c_0 + c_1 DN) \cdot d^2}{E_0 \cos \theta_s} \cdot 100\% ,$$

where c_0 and c_1 are the calibration constants (gain and offset) for the respective sensor, DN are the raw digital numbers, d is the relative sun-earth distance, E_0 is the average solar irradiance, and θ_s is the solar zenith angle.

4.1 Absolute reflectance values

The performance of the atmospheric correction can be evaluated on typical targets from within the image. Selected target spectra have been measured in-field for the HYMAP case. The deviations of the ground sample spectra from the averaged image reflectances are depicted in Figure 3. For the ‘parking lot’ target, both the ATCOR-4 and the CDPC implementation show a slight red edge influence at 740nm, which stems from insufficient adjacency effect correction. At larger wavelengths, the field data are lower than the correction results – an effect which can be due to BRDF, as only one view angle for the imagery was available. This assumption is corroborated by the bare soil sample, where two view angles were available. This sample showed a high deviation between the two angles, leading to up to 30% relative differences. The ground spectra are mostly between the two image samples and thus, the correction seems to be correct despite the angular effects. Less angular influences are visible for the soccer field, where high reflectance accuracy can be found if comparing the image spectra and the ground spectra. Slightly less stable results are found for the pasture sample, but the measurements are still between the two angular HYMAP spectra.

As for the comparison between ATCOR-4 and CDPC, the most significant difference is found at the edges of the water vapor absorption features. The CDPC overcorrects the water vapor influence, which may stem from a too high water vapor retrieval result or from mis-calibration of HYMAP within the water vapor bands (see section 4.5 below). Note that the same overcorrection appears also in ATCOR-4 depending on the selected water vapor processing options.

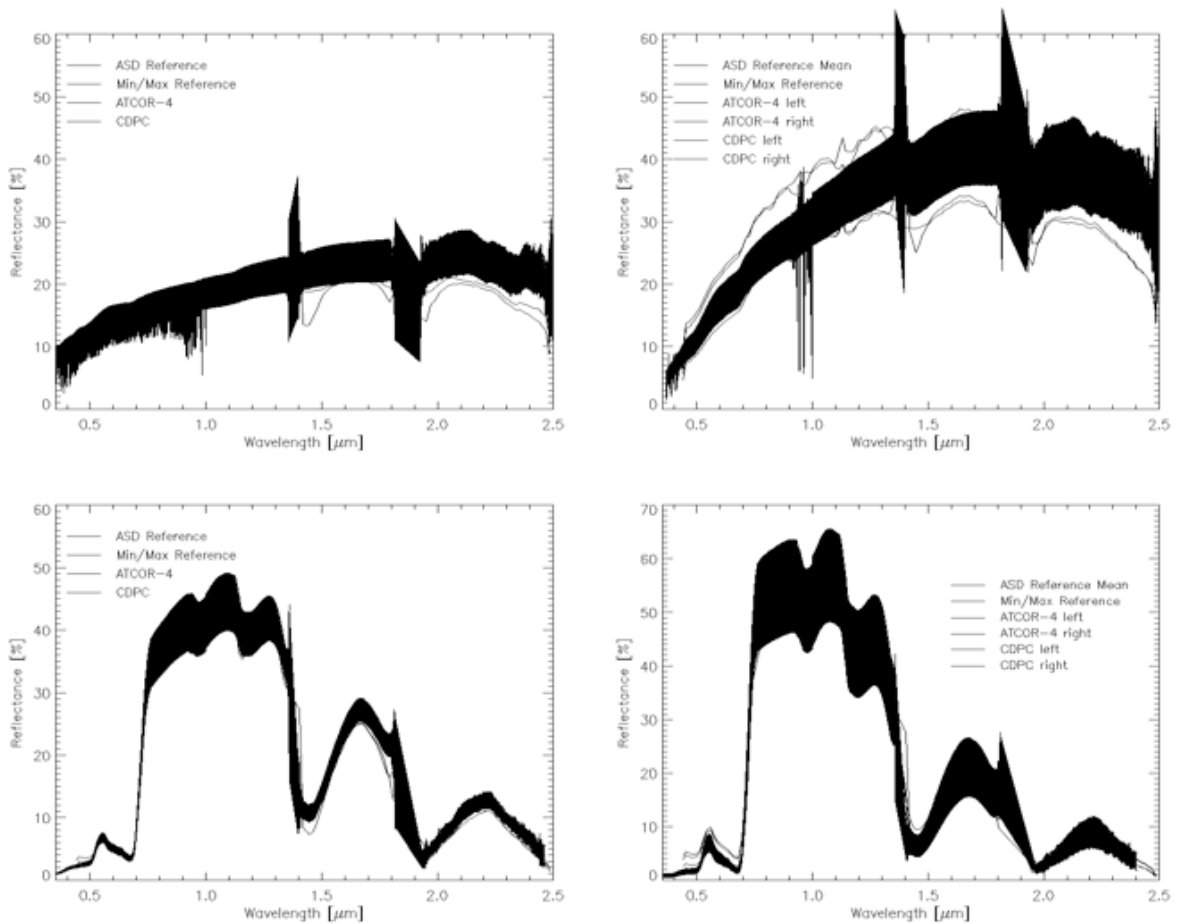


Figure 3 Intercomparison of ATCOR-4/CDPC processed and ground reference spectra. The range of ground reference is given by the colored area. The surface types are: upper left: parking lot, upper right: bare soil, lower left: soccer field, lower right: pasture. Compare positions of measurements in Figure 1 for targets in overlap region (pasture/soil) and those run 2 only (parking lot, soccer field).

4.2 Relative reflectance values (overlap)

The self-consistency of the atmospheric correction can be checked by comparing overlapping areas of two images. For the wide FOV HYMAP case, the differences were significantly higher than for the HYSPEX case, as one would expect. Visual inspection already shows the difference in lightness between the two adjacent image borders (see mosaiced images in Figure 1 and Figure 2, respectively). For the HYMAP case a maximum difference of up to 30% for the most sensitive parameters (i.e., bare soil) is visible in Figure 4. This discrepancy is due to a difference in across track view angles of about -25° to 25° , respectively.

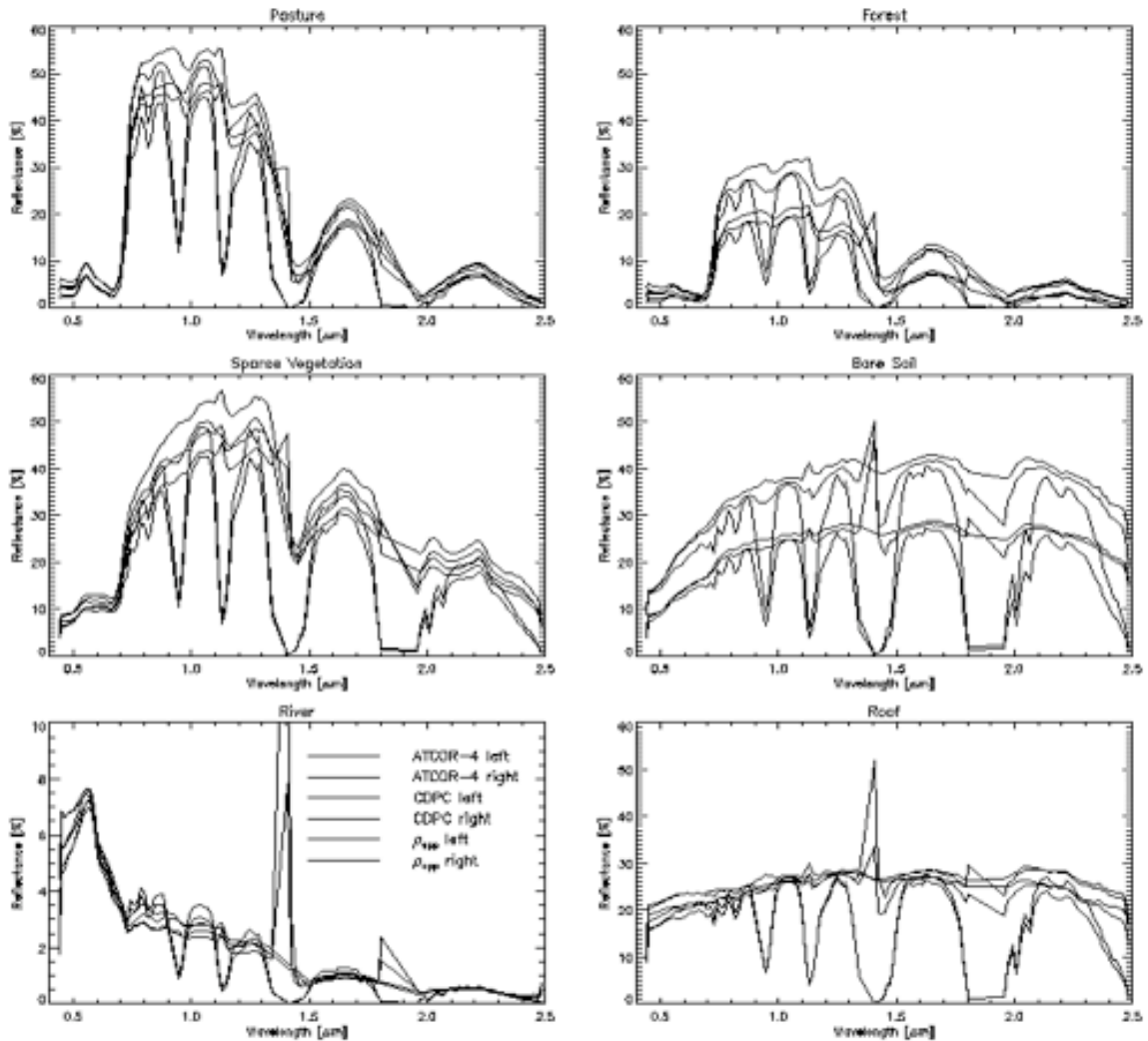


Figure 4 Intercomparison of average bottom of atmosphere reflectance spectra from ATCOR-4, CDPC, and apparent reflectance over selected regions of interest as viewed from two different directions over 6 selected ground targets (from HYMAP data).

The same analysis was made for the HYSPEX scene, where the angular differences are smaller than for HYMAP at about $\pm 6^\circ$. The atmospheric correction outputs on four sample areas of natural surfaces between bare, sandy soil and grassland is depicted in Figure 6. The differences between the two view angles on the same target are lower than for the HYMAP case due to the narrow FOV. The ATCOR-4 correction accounts for the aerosol effect correctly in the visible part of the spectrum and corrects the atmospheric absorption features in the NIR. Some features are not completely removed, as visible in Figure 5. These artifacts have to be attributed to the spectral calibration of the HYSPEX

instrument but they may also be, at least partially, an effect of the limited spectral resolution of the MODTRAN database in ATCOR-4.

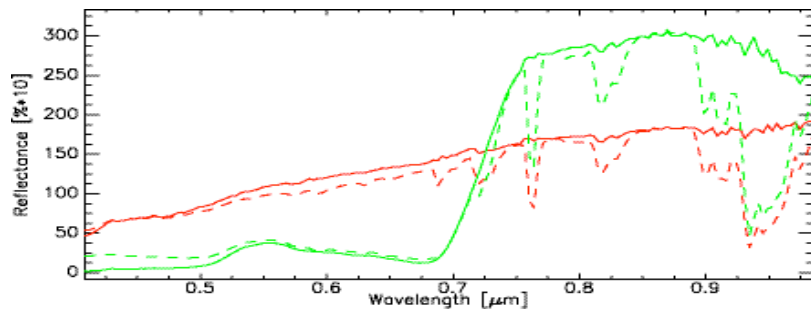


Figure 5 Apparent reflectance (dashed) and corresponding surface reflectance (line) for dense vegetation (green) and bare soil (red).

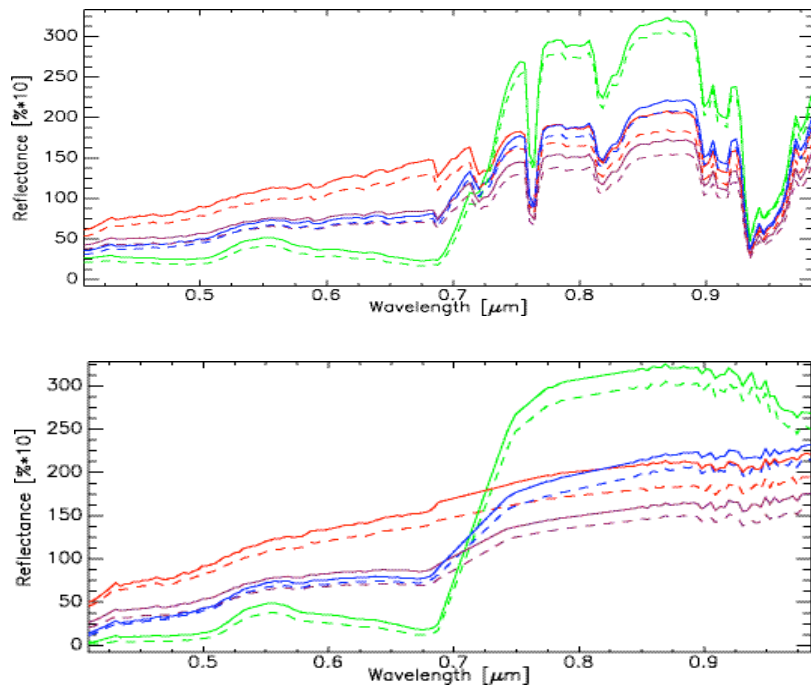


Figure 6 Intercomparison of four HYPSPX Spectra from bare soil to dense vegetation (pasture) in the overlap region. Solid spectra are from the scene 'bio_2' and dashed spectra from 'bio_3'. Top: apparent reflectance, bottom: surface reflectance (all corrections done with ATCOR-4).

4.3 Terrain influence

In rugged terrain, the same target may appear lighter and darker depending on its altitude and solar exposition. The performance of the topographic correction is checked within the image by evaluation of a south-north transect before and after atmospheric/topographic correction. The comparison of north and south slopes reveals a difference in the range of 1% absolute reflectance for visible wavelengths and up to 5% differences in the SWIR spectral range. This corresponds to uncertainties in absolute reflectance for this slight terrain in a range of 20% relative variation of reflectance values. The example is shown in Figure 7. The brightness difference between south and north slope can be seen from the plotted north-south statistics but also directly in the RGB-imagery. After topographic correction, this systematic difference is mostly removed by the ATCOR-4 processor. If an empirical BRDF correction is included, some overcorrection is reduced (see blue lines in Figure 7).

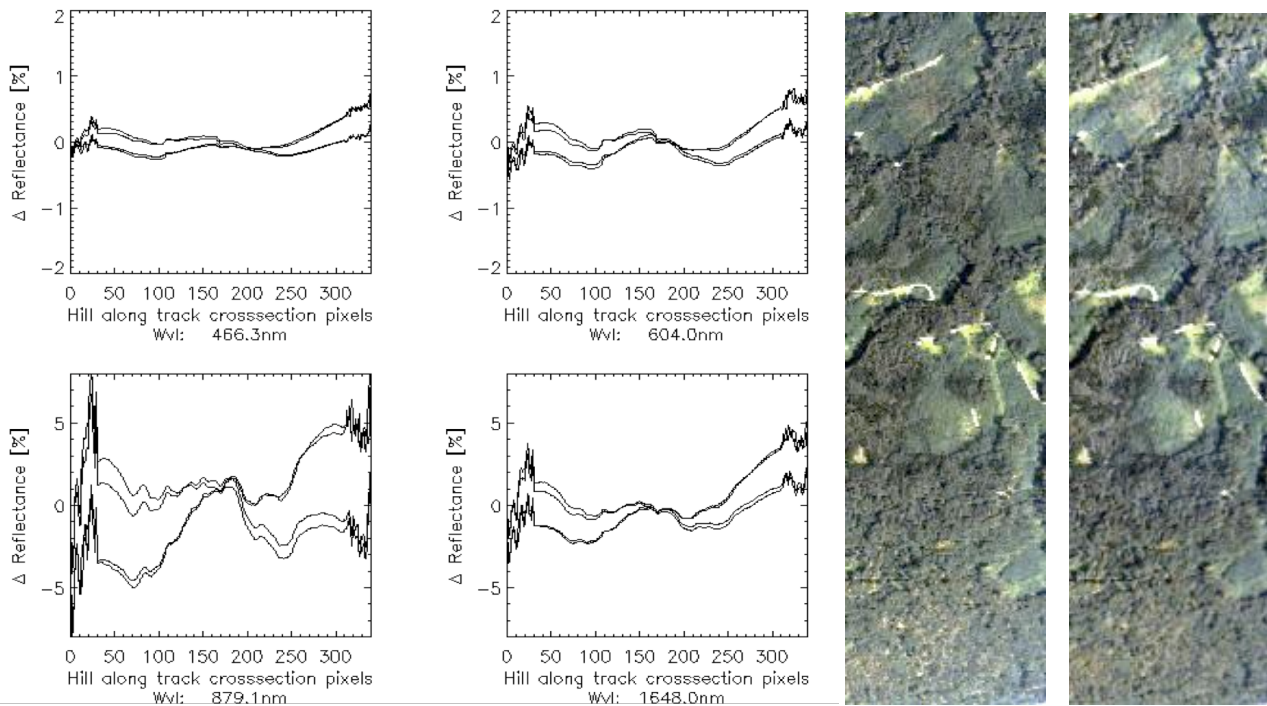


Figure 7 Influence of terrain correction over a north-south slope, deviation from average reflectance of image at four wavelengths. Curves: topographically uncorrected CDPC/apparent reflectance (dashed) and ATCOR-4 corrected (straight line). Blue line: empirical BRDF correction. To the right: image subset for north-south crosssection.

4.4 Aerosols and adjacency

The influence of the adjacency effect can be best shown by evaluation of homogenous targets surrounded by dark or bright background. By taking a cross section in the blue and visible spectral region, the performance of the adjacency correction may be visualized. The respective results can be seen in Figure 8. The significant reduction of the reflectance against non-corrected data in the blue is visible at first. Secondly, a good agreement between ATCOR-4 and CDPC is found. Evaluating extremely bright or dark objects, some differences are visible, which show a stronger correction of adjacency effects by the ATCOR-4 package than in the CDPC software. For HYSPEX data, the adjacency effect is minimal due to the low flight altitude and therefore it is not further analyzed.

Both software packages are able to retrieve aerosol contents and (for ATCOR-4) even the aerosol model automatically from the imagery. The correction results point towards a parameter retrieval which is accurate enough for atmospheric correction – no artifacts could be found in the reflectance spectra which would hint towards aerosol estimates. For the HYMAP case, a 50.9 km visibility for the rural aerosol type was selected by ATCOR-4. In the CDPC implementation, the automatically retrieved averaged MODTRAN visibility was at 74.6 km and 72.2km, respectively over the selected dark pixels. The higher CDPC value is of low probability for that time of the year and this region. Also, the CDPC spectra show a slight undercorrection of the aerosol effect at low wavelengths if compared to ATCOR-4. This significant difference of the CDPC aerosol retrieval, which is based on the same method as ATCOR-4 [13], needs further investigation.

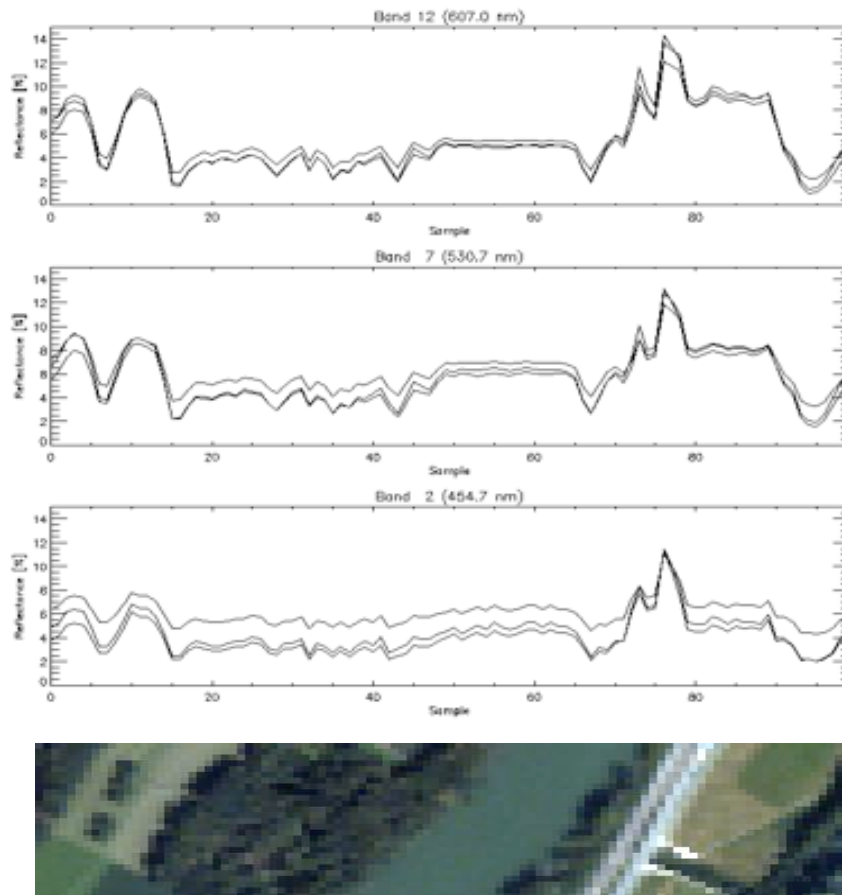


Figure 8 Horizontal profile over river at three different wavelengths, apparent reflectance (dotted), CDPC corrected (dashed) and ATCOR-4 corrected (line).

4.5 Water vapor retrieval outputs

The automatic water vapor retrieval was done for both procedures using the 940 and 1130 nm water vapor absorption bands and using default settings. While ATCOR-4 uses the APDA technology [16] for this retrieval, CDPC is based on the TSR method [14]. Subsets of respective outputs can be seen in Figure 9. The average value for ATCOR-4 was at $19.0 \pm 0.4 \text{ kg/m}^2$, whereas CDPC results were lower at $18.0 \pm 0.4 \text{ kg/m}^2$. The overcorrection artifacts in the surface reflectance spectra had already shown that the total amount of water vapor has been overestimated. This overcorrection may be explained by the fact that the HYMAP data was calibrated by a partially vicarious process, which is very sensitive to the water vapor bands. In addition to the standard routines, a simplified APDA technique similar to the one used in the calibration routine was applied within ATCOR-4 which led to lower water vapor amounts at $17.1 \pm 0.5 \text{ kg/m}^2$ and which improved the spectra significantly. The results as of Figure 3 for ATCOR-4 have been derived using the latter water vapor results – if the physically correct output would have been used, an overcorrection as seen with CDPC would become visible.

Despite the quantitative difference, the two methods perform differently when comparing the outputs visually. The most prominent is the responsivity of the methods to ground reflectance variations. ATCOR-4 shows strong dependencies for its default configuration. These dependencies are reduced if the spectral bands for water vapor retrieval are selected more carefully, which results in a spatial distribution as displayed in the APDA results in the second image of Figure 9. The optimized output of ATCOR-4 and CDPC show quantitatively similar dependencies on the ground reflectance, which are below a 5% level of relative accuracy. However, the APDA methods are known not to work accurately over dark objects. This results in overestimates of water vapor, visible along the forest borders and over the small water pond at the top of the image. This problem could be avoided by interpolation of the water vapor outputs over dark objects.

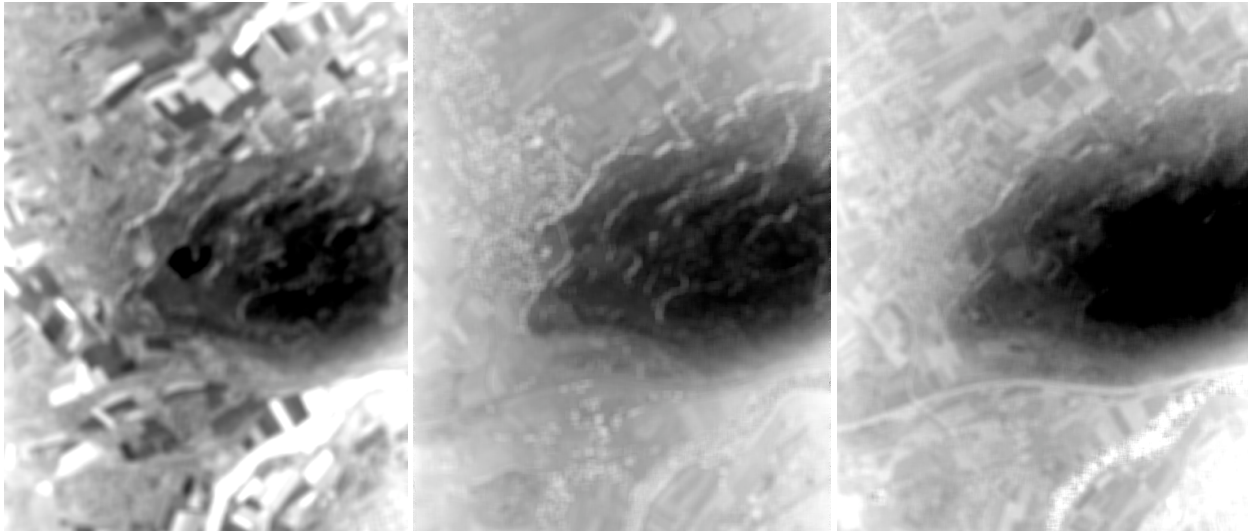


Figure 9 Subset of water vapor retrieval results for the selected methods, left: ATCOR-4 standard settings, middle: optimized ATCOR-4/APDA result, right: CDPC, TSR results; scaled to a range: of 1.7-2.0 for ATCOR-4 outputs and 1.65-1.9 g/cm² for CDPC, respectively.

4.6 BRDF effects

Both software packages offer some limited empirical BRDF correction, which mainly accounts for extreme view angles in terrain. The respective corrections are marginal in the test area and are therefore not any further explained. As already visible in Figure 1, an across-track BRDF effect at angle of 54° off the solar principal plane leads to lightness differences at the image mosaic borders. The effect shows differences in a range up to 18% in absolute reflectance result for this imagery, as can be seen in Figure 4. An even stronger effect would be expected for west-east flights where the variations in the solar principal plane would become visible. The visible BRDF effect is a spectral scale factor with a wavelength dependency due to multiple scattering effects in multidirectional reflectance processes, which is confirmed by the very systematic scaling between the spectra viewed from different angles.

For HYSPEX data, the differences are significantly lower since the angular difference in the overlap region are in a range of 10° instead of about almost 50° in the HYMAP case. Absolute differences of below 5% reflectance can be found if analyzing the data as displayed in Figure 6.

4.7 Computing efficiency

The atmospheric processing of the HYSPEX data using the IDL version of ATCOR-4 (1600x3800pixels x 160 bands) takes 2 hours on a Intel dual core 2.5GHz processor (single core use, Mac OS X). Provided that all input parameters are known, the processing may be started in batch mode and a log file with potential problems is written together with the data. The HYMAP processing took 22 minutes for a scene of 512x2596 pixels and 126 bands on a UNIX machine at 1.5GHz. So, it can be assumed that the processing scales linear with the number of pixels to be processed at a rate of approximately 7.5 Million pixels per minute on current single processor machines.

For the CDPC implementation, the Level1 to Level2 processing times are reported in Table 3. The Linux cluster was composed of 1 master node and 3 worker nodes. Every worker node is a dual-processor Intel XEON at 3.2 GHz. This sub-cluster has its own “work-storage” composed of 5 SAS (Serial Attached SCSI) disks of 140 GB in RAID-0. The processing starts with extracting the necessary data from the cluster archive, where the Level1 images and their metadata are stored in the self-descriptive HDF5 format. Level2 products are packed both in ZIP files and HDF5 files for user distribution or archiving. The Level1 to Level2 processing job was configured from the WWW interface towards the image archive. Once the order is submitted, it is stored in the database system. The master node constantly checks the database system upon new submitted orders and splits the order in elementary jobs that can be executed concurrently and configures the job dependencies. The worker nodes do the actual processing - this master-worker pattern is described in [11]. The total processing time for the atmospheric correction was at 21657 seconds, which corresponds to roughly 6 hours on one processor. This time reduces almost linearly with the number of processors used to approx. 80 minutes, which is still higher than the processing time with ATCOR-4.

Table 3 Cluster timings [seconds] of the Level1 to Level2 processing of the Vordemwald-1 image by the VITO CDPC implementation.

Job type (HYMAP, Vordemwald-1, 126 bands, 2595 scan lines)	Job Count	Total [s]	Total [%]
Extract Level1 IMU/GPS Configuration	1	0	0.00
Extract Level1 IMU/GPS Data	1	0	0.00
Extract Level1 Camera Time	126	3	0.01
Extract Level1 Sensor Configuration	1	0	0.00
Extract Level1 Sensor Data	126	3267	10.76
Extract Level1 Spectral Configuration	1	0	0.00
Extract Level1 GPS/IMU-Camera Sync	1	0	0.00
Sub-total: archive data extraction	257	3270	10.77
Customized Modtran4 simulations	126	9283	30.58
Visibility determination (AOD)	1	279	0.92
Water vapor determination	1	2629	8.66
Atmospheric correction (applying Modtran4 results)	126	9466	31.18
Sub-total: atmospheric correction	254	21657	71.34
Append binary files	2	0	0.00
Append grids	1	3	0.01
Sub-total: data reformatting	3	3	0.01
Orthorectification and viewing and illumination geometry determination	6	289	0.95
Preparation projection and resampling	1	75	0.25
Image projection and resampling	126	1472	4.85
False Color Bitmap Generation	1	7	0.02
Sub-total: geometric correction	134	1843	6.07
File copy	5	170	0.56
Data reformatting: multi-band grid creation	3	123	0.41
Creating ZIP: GIS type data reformatting	252	1303	4.29
Creating ZIP: Level2 Product Package	1	1590	5.24
Creating HDF5: Level2 Product Package	1	393	1.29
Sub-total packaging and distribution	262	3579	11.79
Total number of jobs			910
Total processing time [s]			30359
Actual cluster processing time [s]			6094
Number of Intel XEON CPU's (3.2 GHz)			6

5. CONCLUSIONS

The performance and some limitations of state of the art atmospheric correction software has been investigated in comparison to ground spectra, terrain, and overlapping imagery. It could be shown, that atmospheric absorption features as well as aerosol influences are mostly corrected to a satisfying degree – despite some problems with spectral and radiometric calibration of hyperspectral instruments. Major differences of the correction results have been found in the overlapping regions of the spectra. BRDF effects are apparently affecting the absolute accuracy most significantly and lead to relative differences up to 30% for wide FOV imagery. The differences are smaller for narrow FOV images (as for APEX), but still an influence in a range of 10-20% is to be expected. Due to this huge effect, the absolute accuracy of atmospheric correction may only be measured in reference to directional surface reflectance values. An estimate of the error from the investigated samples points towards a 5% level in absolute reflectance, which reduces to ~3% for low reflectances.

The image-based water vapor and aerosol quantification is appropriate for atmospheric correction purposes. For aerosol retrieval, the results are mostly satisfying and lead to reasonable corrections (despite some apparent implementation differences in the two evaluated routines). The spatial distribution of the water vapor is affected by ground reflectance influences and improvements to this part of the correction are still possible. Also, the band selection for water vapor retrieval needs to be done carefully as unsuited bands will lead to systematic errors and to ground reflectance responsivity.

The atmospheric correction procedures requires still hours of processing time for typical hyperspectral (APEX) scenes. A parallel processing system as implemented in the APEX PAF is thus a major advantage in order to allow operational processing of large campaign data sets in reasonable amounts of time (i.e. a few days).

Future developments in atmospheric correction should strongly focus on BRDF correction of the currently produced bottom of atmosphere reflectances (i.e., equivalent to field-measured HDRF values). It will remain a challenging goal to achieve mosaiced imagery where cross track differences will no longer be visible and will not affect any processing to higher level products.

ACKNOWLEDGEMENTS

We greatly acknowledge the provision of the HYSPEX data by Ivar Baarstad and Trond Løke from Norsk Elektro Optikk (Norway). Silvia Huber, now at WUR, Wageningen, Netherlands, is thanked for providing the HYMAP auxiliary data, and Rolf Richter from DLR Oberpfaffenhofen is acknowledged for the fruitful discussion regarding the ATCOR-4 processing.

REFERENCES

- [1] Nieke, J., Itten, K.I., Debruyn, W. and APEX Team, "The airborne imaging spectrometer APEX: from concept to realisation". In: Proc. 4th EARSeL Workshop on Imaging Spectroscopy, Warsaw, pp. 7 (2005).
- [2] Schläpfer, D. et al., "Optimized Workflow for APEX level 2/3 Processing". In: Proc. 5th EARSeL Workshop on Imaging Spectroscopy., J. Cools (Editor), April 23-25 2007. EARSeL SIG-IS, Bruges, Belgium, pp. 11 (2007).
- [3] Hueni, A., J. Biesemans, K. Meuleman, F. Dell'Endice, D. Schläpfer, D. Odermatt, M. Kneubuehler, S. Adriaensen, S. Kempenaers, J. Nieke and K.I. Itten: "Structure, Components and Interfaces of the Airborne Prism Experiment (APEX) Processing and Archiving Facility". TGARS, vol. 00047, pp. 17 (2008).
- [4] Richter, R. and Schläpfer, D., "Geo-atmospheric processing of airborne imaging spectrometry data. Part 2: Atmospheric/Topographic Correction". International Journal of Remote Sensing, 23(13): 2631-2649 (2002).
- [5] Richter, R., "Atmospheric / Topographic Correction for Airborne Imagery (ATCOR-4 User Guide, Version 4.3)". DLR-IB 565-02/08, available from <http://www.rese.ch/download.html>, pp. 132 (2008).
- [6] Cocks, T., Jenssen, R., Stewart, I., Wilson, I. and Shields, T., "The HyMap™ Airborne Hyperspectral Sensor: The System, Calibration and Performance". In: Proc. 1st Earsel Workshop on Imaging Spectroscopy, EARSeL/RSL, Zürich, pp. 37-42 (1998).
- [7] Baarstad, I., T. Løke, and P.Kaspersen, "ASI, A new airborne hyperspectral imager." In: Proc. 4th EARSeL Workshop on Imaging Spectroscopy-New Quality in Environmental Studies (B. Zagajewski and M. Sobczak, Eds.), Warsaw, Poland, pp 4 (2005).
- [8] Norsk Elektro Optikk, "HYSPEX HyperSpectral Cameras". At <http://www.neo.org/hyspex>, on 3/4/2008 (2008).
- [9] Kötz, B., Sun, G., Morsdorf, F., Ranson, K.J., Kneubühler, M., Itten, K.I. and Allgöwer, B., "Fusion of Imaging Spectrometer and LIDAR Data over Combined Radiative Transfer Models for Forest Canopy Characterization". Rem. Sens. Environ. 106:449-459 (2007).
- [10] Schläpfer, D. and Richter, R., "Geo-atmospheric processing of airborne imaging spectrometry data. Part 1: Parametric Ortho-Rectification Process". International Journal of Remote Sensing, 23(13): 2609-2630 (2002).
- [11] Biesemans, J., S. Sterckx, E. Knaeps, K. Vreys, S. Adriaensen, J. Hooyberghs, K. Meuleman, P. Kempeneers, B. Deronde, J. Everaerts, D. Schläpfer & J. Nieke., "Image processing workflows for airborne remote sensing". In: Proc. 5th EARSeL Workshop on Imaging Spectroscopy, EARSeL, Bruges, Belgium, pp. 8 (2007).
- [12] De Haan, J. F., and Kokke, J. M. M., "Remote sensing algorithm development toolkit I Operationalization of atmospheric correction methods for tidal and inland waters", Netherlands Remote Sensing Board (BCRS) publication, Rijkswaterstaat Survey Dept., Technical Report, pp. 91 (1996).
- [13] Richter, R., D. Schläpfer and A. Müller., "An automatic atmospheric correction algorithm for visible/NIR imagery". International Journal of Remote Sensing, 27(10):2077-2085 (2006).
- [14] Rodger, A.P., "Atmospheric water vapour determination from remotely sensed hyperspectral data". PhD. Thesis, Curtin University of Technology, School of Applied Science., pp. 195 (2002).
- [15] Jupp, D. L. B., "A compendium of kernel & other (semi)empirical BRDF Models". Office of Space Science Applications - Earth Observation Centre, available only as online document, May 2002: www.cossa.csiro.au/tasks/brdf/k_summ.pdf (2000).
- [16] Schläpfer, D., Borel, C.C., Keller, J., and Itten, K.I., "Atmospheric Pre-Corrected Differential Absorption Techniques to Retrieve Columnar Water Vapor". Remote Sens. Environ., 65(3):353-366 (1998).